# Journal of Materials Chemistry A

Accepted Manuscript






ROYAL SOCIETY OF CHEMISTRY

www.rsc.org/materialsA

# Novel Peapod NiO Nanoparticles Encapsulated in Carbon fibers for High-efficiency Supercapacitors and Lithium-ion Batteries

*Yangyang Feng, Huijuan Zhang, Yan Zhang, Yuanjuan Bai, Yu Wang**

The State Key Laboratory of Mechanical Transmissions and the School of Chemistry and Chemical Engineering, Chongqing University, 174 Shazheng Street, Shapingba District, Chongqing City, P.R. China, 400044

E-mail: wangy@cqu.edu.cn; prospectwy@gmail.com

**Abstract**

Nickel oxide is regarded as one of the most promising electrode in energy storage. In this report, a special peapod NiO/C is successfully designed and fabricated for the first time through a simple hydrothermal method by using green glucose as carbon source. This unique structure can not only provide large contact area between electrolyte and active materials so as to promote fast ions and electrons exchange, but also digest possible volume changes during long-time reactions so that it can lead to superior cyclic stability. Importantly, the porous structure can effectively accelerate ions diffusion, further enhancing the electrochemical performances. In this work, our peapod NiO/C exhibits excellent performances in both supercapacitors (SCs) and lithium-ion batteries (LIBs).

**Key words:** Peapod, NiO, Carbon nanotube, Supercapacitors, Lithium-ion batteries

## Introduction

With the rapid increase of energy demand, extensive attention has been concentrated on sustainable energy sources, mainly focusing on unremitting energy supplies, grid-scale energy storage and renewable energy systems.[1, 2] Among all the energy devices, lithium-ion batteries (LIBs) and supercapacitors (SCs) have enticed worldwide interest as two key devices for high power and energy source owing to their high power and energy densities, low-cost, long lifespan, environmental friendliness and safety.[3, 4] As for supercapacitor, the next-generation energy storage device, which provides high power and energy densities as well as long cycle life, has been widely used in the portable electronics and various microdevices.[5-7] However, it still suffers from poor reversibility and rate performances derived from the redox kinetics, which is confined by the speed of electron and ion transfer.[8, 9] Lithium-ion battery, the crucial bridging medium among clean energies, is considered as one of the most promising power systems owing to the high power density, long cycle life and low cost.[10, 11] Nevertheless, it also experiences lots of serious problems, such as agglomeration and pulverization of electrode materials as well as the dramatic decline in specific capacity.[12, 13] To our knowledge, the energy and power densities of the electrical energy storage systems, normally SCs and LIBs, are strongly linked to electrode materials. In the last decades, metal oxides, especially transition metal oxides, like $MnO_2$, $Co_3O_4$, NiO, $MoO_2$, have been extensively discovered as effective electrode materials because of their high specific capacitance and capacity for both SCs and LIBs, respectively.[14-18] Among the transition metal oxides, nickel oxide (NiO) has arrested massive research interests for their plenty of applications, magnetic materials[19], catalyst[20] and gas sensors[21] for instance. Specially, it has been widely applied in SCs electrode and LIBs anode. On the one hand, NiO has a high theoretic capacity (717 mAh/g for LIBs and 2584 F/g for SCs) and high volumetric energy density (~ 5.8 times over graphite).[22, 23] On the other hand, it possesses low toxicity and cost as well as superior safety when

compared with other transition metal oxides.[24] Unfortunately, the poor electrical and ionic conductivity of NiO are somewhat unsatisfied because they can rapidly depress the electrochemical performances.

In order to remit the encountered issues existing in NiO, many methods are applied, including reducing the size of active materials to nanoscale, synthesizing carbon-coated or carbon-related materials as well as doping with foreign atoms.[25, 26] To our knowledge, nano-sized materials can cut down both the ion' and electron' fast diffusion pathways as well as promote close contact between electrode and electrolyte, which can do benefit to the electrochemical performances. [27-29] However, nanoscale materials can easily get aggregation and pulverization, which results in poor cyclic stability. Thus, it is urgent to design and fabricate novel nanocomposites to solve the above problems. Among various nanostructures, one-dimensional (1D) nanoarchitectures stand for one of the most promising structures, mainly because of their attractive properties and applications in plenty of fields.[30] In the last decades, different NiO nanostructures, such as nanotubes[31], nanowires[32] and nanocones[33] have been achieved to enhance the performances of energy storage. Particularly, tubular nanoarchitecture can be taken as intriguing 1D structure due to its fantastic features.[34] Nevertheless, the 1D nanostructures are relatively simple and can not meet the demand of practical application. Consequently, designing and synthesizing novel complex structures with other materials included, especially conductive materials, is expected for more opportunities to enhance the electrochemical properties. Among the designed 1D nano-materials, peapod-like structural materials are regarded as one of the most attractive and significant candidates for energy storage.[28, 35]

Herein, we devise and synthesize a novel peapod NiO nanoparticles encapsulated in carbon fibers by a new and general strategy. In this method, we use 1D α-$Ni(OH)_2$ nanowire as precursor and sacrificial templates, green glucose as carbon source. With the help of hydrogen-bonding, the glucose polymer is strictly fixed onto the surface of α-$Ni(OH)_2$ nanowires. After high-temperature calcination and air oxidization, α-$Ni(OH)_2$ nanowires are transferred into NiO nanoparticles while glucose polymer is changed into carbon fibers, which looks like peapod. This peapod-like structure, on one hand, can ensure fast ion and charge transfer due to the 3D conductive network constructed by carbon fibers. On the other hand, the interspaces between each NiO nanoparticles can effectively buffer possible volume expansion during electrochemical reactions as well as prohibit active materials from aggregating and agglomerating. More importantly, the porous structure derived from lots of substances loss can not only accelerate efficient contact between active materials and electrolyte, but also promote ions' and electrons' diffusion. Therefore, our special peapod NiO/C can strikingly enhance the electrochemical performances in both SCs and LIBs.

**Results and Discussion**

The overall synthesis process is illustrated in Sch. 1. At first, we fabricated α-$Ni(OH)_2$ nanowires through a general and feasible method. Similar to our previous reports, we use glucose as low-cost and environmentally friendly carbon source. Under the action of hydrogen-bonding between α-$Ni(OH)_2$ nanowires and glucose, the polymer tightly wrapped around the surface of the precursor. Finally, the novel peapod NiO nanoparticles encapsulated in graphitized carbon fibers were synthesized through high-temperature calcinations in Ar followed by oxidization in $O_2$. This NiO composite with unique morphology can be considered as high-efficiency electrodes in both

SCs and LIBs.

Typical characterizations of as-prepared α-$Ni(OH)_2$ nanowires are presented in Fig. 1. Low-magnification scanning electron microscopy (SEM) image and magnified SEM image are shown in Fig.1a and 1b, from which we can see that large-scale α-$Ni(OH)_2$ nanowires can be easily synthesized with several micrometers in length. In the transmission electron microscopy (TEM) image (Fig. 1c), the width of the precursor is estimated to be 20-40 nm. The X-ray diffraction data (XRD) is revealed in Fig. 1d, where all the diffraction peaks from 5-90 degrees are well-matched with the pure α-$Ni(OH)_2$ (JCPDS No. 41-1424), verifying that the pure and single crystalα-$Ni(OH)_2$ nanowires can be easily fabricated in a uniform way. Under the suitable in situ carbon coating followed by calcinations in Ar atmosphere, grandscale peapod Ni/C can be feasibly accessible. The relevant characterizations are also provided. As displayed in Fig. S1a (supporting information), the peapod structure, with numerous nanoparticles in line in the graphitized carbon fibers, can be distinctly observed. The XRD pattern is also presented in Fig. S1b, where the peaks varying from 10 to 90 $^{o}$ are in correspondence with the pure Ni (JCPDS No.87-0712). Noteworthily, there exists a small peak at ~26.6 $^{o}$ that it is derived from the graphitized carbon under high temperature calcinations.

After the second annealing in air, peapod NiO/C can be largely fabricated due to the purity and homogeneity of the precursor and the intermediate products. It is observed in Fig.2a, peapod morphology is prepared evenly and uniformly. In the amplified SEM image (Fig.2b) as well, peapod NiO/C is distinctly detected with a plenty of nanoparticles strictly confined in line inside of the graphitized carbon nanotube. Furthermore, even under 5 kV of scanning electron beam, nanoparticles can be clearly seen even dotted in the carbon fibers, indicating the ultrathin carbon layers wrapping around nanoparticles, well succeeded to the precursor. Fig. 2c is the XRD data of the final samples. It is revealed that the peaks from 30-90 degree are index to the pure NiO (JCPDS No.78-0643). Herein, we can also capture a weak peak at around 26.6$^{o}$， suggesting the well graphitization of the final composite even through annealing in air. To further confirm the graphitization of our peapod NiO/C, Raman spectroscopy (RS) is also essential. G band refers to the planar vibration of sp2-type carbon atoms (indicating graphitized carbon), while D band stands for amorphous and disordered carbon.[36, 37] Shown in Fig. S2 (supporting information), the ratio of G band/D band is ~1, implying that the well-graphitized of as-fabricated composites are achieved at the appropriate conditions. To our knowledge, graphitized carbon wrapping around the active materials can effectively enhance the electronic conductivity, prevent the nanoparticles from peeling off and buffer the possible volume changes during long electrochemical cycles, so it can improve the electrochemical performances. The carbon content is pretty significant in carbon-related materials. In order to evaluate the carbon content, TG measurement is carried out. As shown in Fig. S3 (supporting information), the carbon content of this composite is ~ 6.5 % calculated from the measurement after 150 $^{o}$C as there is a bit of water volatilization below 150 $^{o}$C.[38, 39] The small amount of carbon can hardly reduce the capacity/capacitance of the active materials. On the contrary, it can efficiently lower the charge transfer resistance since electron can be rapidly and facilely diffused between electrolyte and the active materials, thus effectively increasing the delivered specific capacity. Via the corresponding X-ray energy dispersive spectrum (EDS) analysis in Fig. 2d, it is observed that Ni, O and C are existed in the composite, with the ratio of Ni and O ~ 1:1, which exactly suggests the NiO nanoparticles combining with the XRD pattern in Fig. 2c. With the purpose of investigating the elements' distribution in the final

composite, selected area's elemental imaging of EDS is carried out. Revealed in Fig. S4 (supporting information), the Ni&O are uniformly confined in the graphitized carbon nanotubes. Moreover, the evenly C distribution confirms the well-distributed coating on NiO nanoparticles.

Transmission electron microscopy (TEM) is an efficient means to analyze the detailed structure in micro-scale. As is the TEM image of the final samples in Fig. 3a, numerous peapod NiO/C assuredly provides clear evidence that the peapod NiO/C can be synthesized on a large scale, which is the necessary condition for practical applications. In the amplified TEM image of Fig. 3b, the peapod structure is clearly presented. And in Fig. 3c, many nanoparticles stay in line in the graphitized carbon fibers with an average diameter of 5 nm. Furthermore, the inter-space of ~ 2 nm between each nanoparticle helps to buffer the volume expansion during electrochemical reactions, especially to oxides, which can efficiently maintain the architectural integration so as to enhance the cyclability of active materials. The HRTEM image in Fig. 3d provides the crystal structure of NiO nanoparticles. It is observed that the lattice spacing between crystal planes is 0.104, in correspondence to the (400) crystal plane of pure NiO, further affirming it NiO combining with the XRD and EDS data.

Nitrogen adsorption and desorption isotherms (BET) is an indispensable tool to estimate both the specific surface area and porous distribution. As revealed in Fig. 4, the specific surface area obtained through $N_2$ adsorption and desorption profile is ~ 156.208 $m^2/g$. The porous distribution (Fig. 4, inset) derived from Barrete-Joyner-Halenda (BJH) analysis shows that the pore size in the peapod ranges form 1.8-4 nm, mainly concentrated on 1.8 nm, suggesting that the pervasive porous structure can be prosperously synthesized via appropriate conditions owing to generous substances loss. To our knowledge, the large surface area can not only offer more active area for electrochemical reactions, but also facilitate the contact between electrolyte and the active materials. More importantly, the porous structure can effectively accelerate the ion' and electron' fast exchange through electrolyte and active nanoparticles, further enhance the electrochemical properties.[10, 40]

NiO is considered as a multi-functional materials applied in both SCs and LIBs. In order to estimate its promising use of peapod NiO/C in SCs, a series of electrochemical tests are carried out. The cyclic voltammetry curves (Fig. 5a) of our peapod composite were tested at various scan rates from 5 to 100 mV/s within the potential range of 0-0.6 V. Obviously, there exists a couple of apparent redox peaks in every CV curves, which may be based on the formation of NiOOH on the surface of the active materials when reacted in alkaline solutions. The related reaction is represented in the following equation[41, 42]: $NiO + OH^- \longrightarrow NiOOH + e^-$. Furthermore, it is also observed in Fig. 5a that as the scan rate increases, the current density gradually improves. Besides, a slightly shifts of the oxidation and reduction peak potential can be seen at the higher rates, which may result from the electric polarization and irreversible reactions when the scan rate increases.[43] A set of galvanostatic discharge plots in a potential range of 0-0.5 V are shown in Fig. 5b. It reveals that the specific capacitance of our peapod composite can reach up to 2048 F/g at the current density of 1 A/g on the basis of the discharge curves, which is pretty higher than most of the NiO-based materials.[8, 44, 45] Even at such a high rate of 40 A/g, the specific capacitance is as high as 1573 F/g. Fig. 5c displays the corresponding rate properties from 1 A/g to 2, 5, 10, 20, 30 and 40 A/g. Consistently, the specific capacitance changes from 2048 F/g to 1921, 1815, 1747, 1670, 1617 and 1573 F/g, respectively. The cyclic stability is an important indicator for high-efficiency SCs, as shown in Fig. 5d, there is almost no attenuation (~3%) in the specific

capacitance even running for 8000 cycles at the current density of 20 A/g, suggesting the excellent stability of our novel peapod NiO/C.

To further demonstrate the superiorities of the elaborate architecture, the electrochemical behaviors of NiO nanoparticles are also tested for comparison. The morphology of NiO nanoparticles is revealed in Fig. 6a. And the CV profiles of both peapod NiO/C and NiO nanoparticles are displayed in Fig. 6b, from which we can see that the peapod NiO/C exhibits the increased current when tested at the same scan rate of 20 mV/s, indicating the enhanced performances of our peapod composite. Based on the galvanostatic discharge plots of Fig. 6c, peapod NiO/C demonstrates a high specific capacitance of 1670 F/g, while the NiO nanoparticles exhibits relative low specific capacitance of 679 F/g, which suggests that our peapod NiO/C is more desirable for SCs. The cyclic stability of NiO nanoparticles is presented in Fig. 6d. It is observed that NiO nanoparticles show a much poor specific capacitance and a rapid decay in the following cycles especially after 2000 cycles. The superior performances indeed result from our novel structure design. To gain more insight into our structural advantages, we further to compare our composite to other reported NiO-based materials in the previous literatures (shown in Table 1)[8, 22, 45-51]. As presented, our peapod NiO/C possesses excellent electrochemical properties in SCs among others with different morphologies, significantly implying the superiorities of our peapod structure. In one aspect, the unique 1D morphology with nano-scaled size can help to shorten pathways for both ions and electrons and enlarge the contact area between electrolyte and active materials, leading to high specific capacitances. In another aspect, the novel carbon-related materials of active materials wrapped inside with an interval between each active nanoparticles can effectively digest volume changes and protect nanoparticles from aggregation and peeling off during long-term running, bringing in superior cyclic stability. Besides, the porous structure that the peapod NiO/C possesses can promote fast ion and electron exchange, further enhancing the electrochemical performances.

To further study the electrochemical behavior of our final composite, electrochemical impedance spectroscopy (EIS) is also conducted, which was tested with the frequency range of 0.01 Hz to 100 Hz at the AC perturbation amplitude of 5 mV. The Nyquist plots of peapod NiO/C before and after electrochemical reactions and the corresponding equivalent circuit are shown in Fig. S5 (supporting information). It is observed that our peapod electrode are well contacted with the current collector due to a slightly increase in internal resistance ($R_s$) after 8000 cycles. Furthermore, the charge transfer resistance ($R_f$, calculated by the semicircle in the high-frequency region) is 1.30 Ω in the initial cycle. Notably, even after operating for 8000 cycles, the $R_f$ lightly changes from 1.30 to 1.75 Ω, significantly revealing that our peapod structure can remarkably improve the electroactive surface area and electroconductivity.

To evaluate the asymmetric supercapacitor performances, asymmetric supercapacitor(ACS) was assembled by utilizing carbon and peapod NiO/C as negative and positive electrode, respectively (NiO/C//AC-ACS). Fig. 7a presents the CV curves of ACS performed in a potential window of 0 - 1.6 V at the scan rates ranging from 10 to 200 mV/s. Different from the peapod NiO/C electrode, the ACS devices shows almost rectangular CV plots rather than apparent redox peaks, indicating the desirable capacitive behavior. In addition, the current in the CV curves increases as the scan rate magnifies without obvious distortion, suggesting the ideal rapid charge/discharge properties for electric devices.[52, 53] The galvanostatic charge/discharge profiles are tested at various current densities from 1 to 20 A/g with the potential range of 0-1.6 V. As observed in Fig. 7b, the nearly

linear correlation and the highly symmetrical shape further exhibit the satisfied capacitive properties of the NiO/C//AC-ACS. Based on the discharge curves in Fig. 7b, the corresponding rate performances are calculated in Fig. 7c. As revealed, our ACS devices demonstrate maximum specific capacitance of 235, 218, 201, 189 and 174 F/g when measured at the current density of 1, 2, 5, 10 and 20 A/g, separatively, with ~ 26 % loss, further verifying the excellent rate properties of our peapod composite. Cyclability is also a crucial factor for SCs, then the cyclic stability is measured through galvanostatic charge and discharge from 0 to 1.6 V at the current density of 10 A/g (Fig. 7d). As expected, our peapod NiO/C//AC-ACS exhibits outstanding stability with a capacitance retention of ~96.7 % even running for 3000 cycles. These observations can indeed confirm that our novel peapod NiO/C could enhance the electrochemical performances, especially the rate properties and cyclic stabilities.

Apart from SCs, our peapod NiO/C can be also considered as high-efficiency anode in LIBs. To evaluate its properties, many measurements are conducted. Fig. 8a is the galvanostatic charge/discharge profiles performed at a constant current of 0.5 A/g over the voltage range of 0.01 to 3 V *vs.* $Li/Li^+$. Notably, the initial discharge capacity can reach up to 1723 mAh/g, much higher than the theoretical capacity of NiO (717 mAh/g), which may be ascribed to the formation of solid electrolyte interface (SEI) film and the porous structure.[23, 54] From the second cycle, the capacity decreases to 1193 mAh/g and remains stable even for 200 cycles with about 97.3% retention. Herein, a large voltage plateau is visible at ~0.65 V, which may be derived from the reduction of NiO to Ni in the electrochemical reactions.[55] In order to test the rate performances, the current densities continuously increase from 0.5 A/g to 1, 5, 10, 20 and 40 A/g with the specific discharge capacities change from 1193 mAh/g to 1017, 915, 821, 712 and 569 mAh/g, separatively (Fig. 8b). Finally, after running for 300 cycles at various current densities, the capacity can return to 1168 mAh/g when the current back to 0.5 A/g, indicating the outstanding rate properties of peapod NiO/C. Taking more insight into the rate performances, galvanostatic charge/discharge tests at different current densities are carried out. As shown in Fig. 8c, owing to the dynamic limitation, the separation plateaus in charge/discharge curves gradually enlarge as the current densities increase, similar to the reported NiO-based materials.[56, 57] More importantly, the specific capacity is as high as 763 mAh/g even at such high current density of 20 A/g, implying the superior rate properties of the peapod composite. The coulombic efficiency of our peapod NiO/C is also presented in Fig. 8d, which is calculated by the ratio of charge and discharge capacities. It is observed that our peapod composite exhibits high coulombic efficiency of nearly 100% for 200 cycles running at the current density of 0.5 A/g. All the observations revealed above can absolutely verify the superiority of our peapod composite in LIBs. To highlight the peapod structure design, the cyclic stability of pure NiO nanoparticles is provided. From Fig. S6 (supporting information), we can detect that the pure NiO nanoparticles exhibit a much poorer specific capacity in the first two cycles and a rapid decay in the subsequent ones, remarkably implying the excellent cyclic stability of our peapod structure. In addition, we also compare our composite to other NiO-based materials reported in the previous literatures. As shown in Table 2, our peapod NiO/C still demonstrates enhanced electrochemical performances among other NiO-based materials with different morphologies,[55, 58-66] further confirming the structural preponderances of peapod. To affirm the structural stability, we revisit the peapod NiO/C after running for 200 cycles. The SEM image (Fig. S7, supporting information) shows that the peapod structure is well-maintained even after long time reactions, fully verifying the unexceptionable

stability of our peapod morphology. In order to verify the great electrical conductivity of our peapod NiO/C, the Nyquist plots and the corresponding equivalent circuits of both peapod NiO/C and NiO nanoparticles are presented in Fig. S8 (supporting information). It is observed that the charge transfer impedance of peapod NiO/C is much lower than that of pure NiO nanoparticles due to the smaller high-to-medium-frequency semicircle in the Nyquist plots. More importantly, after long time electrochemical reactions, charge-transfer resistance of our peapod NiO/C slightly increases ~ 20 Ω while that of NiO nanoparticles augments ~100 Ω, significantly verifying that peapod structure with graphitized carbon wrapping outside and NiO nanoparticles encapsulated inside can definitely enhance the electronic conductivity and then promote the Li-ion storage performance. Based on the above results, it is believed that the designed peapod NiO/C is desirable for high-efficiency electrode in energy storage.

**Conclusion**

Novel peapod NiO nanoparticles encapsulated in carbon nanotubes are firstly designed and synthesized through a general hydrothermal method followed by two-step calcinations. The unique 1D peapod morphology possesses numerous prominent superiorities, such as huge specific surface area, porous structure and high electroconductibility. Therefore, the peapod NiO/C exhibits outstanding electrochemical performances in both SCs and LIBs. When applied as electrode in SCs, the peapod composite demonstrates high specific capacitance of 2048 F/g at 1 A/g and excellent cyclic stability (~97% retention after 8000 cycles). When evaluated as LIBs anode, our peapod NiO/C exhibits superior rate performances and enhanced cyclability (~97% retention after 200 cycles). It is believed that this unique design can broaden the scope for future researches among lots of fields.

**Experimental Section**

**Materials**: All chemicals or materials were utilized directly without any further purification before use: nickel sulfate ($NiSO_4$, 99.9%, Aldrich ), sodium hydroxide (NaOH, 99.9%, Aldrich), glucose (Cica-Reagent, Kanto Chemical).

**Preparation of α-Ni(OH)$_2$ nanowires:** In a typical synthesis of α-$Ni(OH)_2$, $NiSO_4$ 9.8 mmol, NaOH 9.8 mmol, 30 mL deionized water were mixed step by step under strong stirring. Then, after stirring for 15 min, the precursor solution changed into green solution. Subsequently, we transferred the mixture into autoclave with a volume of 50 mL at 160 $^oC$ for 3 h. When the autoclave cooled naturally to room temperature in air, green samples were collected and washed by using deionized water and pure ethanol. After that, the as-prepared samples were dried in oven at 60 $^oC$ overnight to remove the absorbed water and ethanol.

**Preparation of peapod-like NiO/C nanocomposites:** α-$Ni(OH)_2$ nanowires (100 mg) were added into 25 mL deionized water together with 1M glucose aqueous solution (5 mL). The uniform solution was then transferred into a Teflon-lined autoclave of 50 mL at 180 $^oC$ for 8 h. Subsequently, the composite was cleaned and washed by three times of D.I. water and one time of ethanol, and then dried in oven at 60 $^oC$ overlight. Afterwards, the dried samples were calcined in tube furnace in Ar at 700 $^oC$ for 200 min. Finally the intermediate samples were annealed again at 250 $^oC$ for 200 min in air to oxidize the previously formed Ni to NiO.

**Material characterization:** The fabricated composites are characterized by the following instruments: X-ray diffractometer (XRD, Cu Kα, Bruker D8 Advance); Field-emission scanning electron microscope (SEM, 5kV, JSM-7800F) equipped with an energy dispersive spectrometer (EDS) analyzer; Transmission electron microscope (TEM, Philips, Tecnai, F30), BET surface-area and pore-size analyzer (Quantachrome Autosorb-6B); Raman Microscope (RENISHAW Invia, UK, voltage (AC) 100-240V, Power 150W) and thermogravimetric analyzer (TGA, Mettler Toledo).

**Electrochemical testing:** For lithium-ion battery test, the working electrodes are prepared by peapod NiO/C with the loading mass of 1.1-1.3 mg/cm$^2$ covered on the Cu foil. The electrode consists of 85wt.% peapod NiO/C, 10 wt.% carbon black and 5 wt.% polyvinylidene fluoride (PVDF) with a few drops of N-methyl pyrrolidinone (NMP). The mixture was stirring for at least 1 day and spread on 12 mm Cu foil. Subsequently, the Cu foil with samples was dried in vacuum at 80$^oC$ for 24 h. The half-cells were constructed in argon-filled glove box under a pressure of 20 Mpa. We use the pure Li foil (99.9%, Aldrich) as the counter electrodes, Cellgard2400 as the separator, and 1 M $LiPF_6$ in ethylene carbonate (EC)/dimethyl carbonate (DMC) (v/v = 1:1) as the electrolyte. The galvanostatic charge-discharge were tested on a Neware battery testing system in the voltage range of 0.01-3.0 V.

Supercapacitors test was measured on a electrochemical workstation (CHI660E) by using a three electrode setup, including peapod-like NiO/C as working electrode, a Pt foil as counter electrode, a saturated calomel electrode (SCE) as reference electrode, and 1 M KOH aqueous solution as the working electrolyte. The cyclic voltammetry (CV) and galvanostatic charge/discharge measurements were carried out in the potential range of 0-0.6 V. Asymmetric capacitors (ACS) were performed in two-electrode test system in 1 M KOH aqueous solution. ACS was assembled using peapod-like NiO/C and active carbon (AC) as positive and negative electrons, respectively.

The specific capacitance of peapod-like NiO/C was calculated from the charge–discharge curves based on the following equation:

$$C_s = \frac{I \times \Delta t}{m \times \Delta V}$$

where Cs (F/g) is the specifi c capacitance; I(A) refers to the discharge current, Δ V(V) represents the potential change within the discharge time Δ t(s), and m(g) corresponds to the total weight of the peapod-like NiO/C**.**

**Acknowledgements**

This work was financially supported by the National Natural Science Foundation of China (NSFC, Grant No. 21373280，21403019), Thousand Young Talents Program of the Chinese Central Government (Grant No.0220002102003), Fundamental Research Funds for the Central Universities (0301005202017), Beijing National Laboratory for Molecular Sciences (BNLMS), and Hundred Talents Program at Chongqing University (Grant No. 0903005203205).

**Supporting Information Available:** More SEM, EDS, XRD data are available in the supporting information for this paper.

**References**


1. M. Armand and J. M. Tarascon, *Nature*, 2008, **451**, 652-657.
2. H. B. Gray, *Nat Chem*, 2009, **1**, 7-7.
3. P. G. Bruce, B. Scrosati and J.-M. Tarascon, *Angew. Chem. Int. Ed.* , 2008, **47**, 2930-2946.
4. C. Z. Yuan, H. B. Wu, Y. Xie and X. W. Lou, *Angew. Chem. Int. Ed.* , 2014, **53**, 1488-1504.
5. Z. Fan, J. Yan, T. Wei, L. Zhi, G. Ning, T. Li and F. Wei, *Adv. Funct. Mater.*, 2011, **21**, 2366-2375.
6. H. Wang, H. S. Casalongue, Y. Liang and H. Dai, *J. Am. Chem. Soc.*, 2010, **132**, 7472-7477.
7. L. Bao, J. Zang and X. Li, *Nano Lett.*, 2011, **11**, 1215-1220.
8. C. H. Wu, S. X. Deng, H. Wang, Y. X. Sun, J. B. Liu and H. Yan, *ACS Appli. Mater.Inter.*, 2014, **6**, 1106-1112.
9. A. S. Adekunle, K. I. Ozoemena, B. B. Mamba, B. O. Agboola and O. S. Oluwatobi, *Int. J Electrochem. Sci.*, 2011, **6**, 4760-4774.
10. Y. Feng, H. Zhang, L. Fang, Y. Ouyang and Y. Wang, *J. Mater. Chem. A*, 2015, **3**, 15969-15976.
11. Y. Y. Feng, H. J. Zhang, Y. P. Mu, W. X. Li, J. L. Sun, K. Wu and Y. Wang, *Chem-Eur J*, 2015, **21**, 9229-9235.
12. H. J. Zhang, Y. J. Bai, Y. Zhang, X. Li, Y. Y. Feng, Q. Liu, K. Wu and Y. Wang, *Sci Rep*, 2013, **3**.
13. S. R. Gowda, A. L. M. Reddy, M. M. Shaijumon, X. Zhan, L. Ci and P. M. Ajayan, *Nano Lett.*, 2011, **11**, 101-106.
14. J. Zhu and J. He, *ACS Appli. Mater.Inter.*, 2012, **4**, 1770-1776.
15. X. H. Xia, J. P. Tu, Y. Q. Zhang, J. Chen, X. L. Wang, C. D. Gu, C. Guan, J. S. Luo and H. J. Fan, *Chem. Mater.*, 2012, **24**, 3793-3799.
16. L. Yang, S. Cheng, Y. Ding, X. B. Zhu, Z. L. Wang and M. L. Liu, *Nano Lett.*, 2012, **12**, 321-325.
17. T. Brezesinski, J. Wang, S. H. Tolbert and B. Dunn, *Nat. Mater.*, 2010, **9**, 146-151.
18. S. Dong, X. Chen, L. Gu, X. Zhou, H. Xu, H. Wang, Z. Liu, P. Han, J. Yao, L. Wang, G. Cui and L. Chen, *ACS Appli. Mater.Inter.*, 2011, **3**, 93-98.
19. V. Salgueiriño-Maceira, M. A. Correa-Duarte, M. Bañobre-López, M. Grzelczak, M. Farle, L. M. Liz-Marzán and J. Rivas, *Adv. Funct. Mater.*, 2008, **18**, 616-621.
20. D. S. Wang, R. Xu, X. Wang and Y. D. Li, *Nanotechnology*, 2006, **17**, 979-983.
21. G. Mattei, P. Mazzoldi, M. L. Post, D. Buso, M. Guglielmi and A. Martucci, *Adv Mater*, 2007, **19**, 561-564.
22. K. Liang, X. Z. Tang and W. C. Hu, *J. Mater. Chem.* , 2012, **22**, 11062-11067.
23. Y. Feng, H. Zhang, W. Li, L. Fang and Y. Wang, *J Power Sources*, 2016, **301**, 78-86.
24. J. Cabana, L. Monconduit, D. Larcher and M. R. Palacin, *Adv Mater*, 2010, **22**, E170-E192.
25. P. Simon and Y. Gogotsi, *Nat. Mater.*, 2008, **7**, 845-854.
26. Y. Y. Feng, Y. OuYang, L. Peng, H. J. Qiu, H. L. Wang and Y. Wang, *J. Mater. Chem. A*, 2015, **3**, 9587-9594.
27. Y. Y. Feng, H. J. Zhang, Y. Zhang, X. Li and Y. Wang, *ACS Appli. Mater.Inter.*, 2015, **7**, 9203-9210.
28. H. Zhang, Y. Feng, Y. Zhang, L. Fang, W. Li, Q. Liu, K. Wu and Y. Wang, *ChemSusChem*, 2014, **7**, 2000-2006.

29. J. Chen and F. Cheng, *Acc. Chem. Res.*, 2009, **42**, 713-723.
30. Y. N. Xia, P. D. Yang, Y. G. Sun, Y. Y. Wu, B. Mayers, B. Gates, Y. D. Yin, F. Kim and Y. Q. Yan, *Adv Mater*, 2003, **15**, 353-389.
31. S. A. Needham, G. X. Wang and H. K. Liu, *J. Power Sources*, 2006, **159**, 254-257.
32. D. W. Su, H. S. Kim, W. S. Kim and G. X. Wang, *Chem-Eur J*, 2012, **18**, 8224-8229.
33. X. Wang, Z. Yang, X. Sun, X. Li, D. Wang, P. Wang and D. He, *J. Mater. Chem.* , 2011, **21**, 9988-9990.
34. S. J. Peng, L. L. Li, Y. X. Hu, M. Srinivasan, F. Y. Cheng, J. Chen and S. Ramakrishna, *Acs Nano*, 2015, **9**, 1945-1954.
35. Y. Wang, H. J. Zhang, L. Lu, L. P. Stubbs, C. C. Wong and J. Y. Lin, *Acs Nano*, 2010, **4**, 4753-4761.
36. J. Ha, S.-K. Park, S.-H. Yu, A. Jin, B. Jang, S. Bong, I. Kim, Y.-E. Sung and Y. Piao, *Nanoscale*, 2013, **5**, 8647-8655.
37. E. Flahaut, F. Agnoli, J. Sloan, C. O'Connor and M. L. H. Green, *Chem. Mater.*, 2002, **14**, 2553-2558.
38. M. M. Rahman, S.-L. Chou, C. Zhong, J.-Z. Wang, D. Wexler and H.-K. Liu, *Solid State Ionics*, 2010, **180**, 1646-1651.
39. S. Vijayakumar, S. Nagamuthu and G. Muralidharan, *ACS Sustainable Chem. Eng.*, 2013, **1**, 1110-1118.
40. Y. Huang, X.-l. Huang, J.-s. Lian, D. Xu, L.-m. Wang and X.-b. Zhang, *J. Mater. Chem.* , 2012, **22**, 2844-2847.
41. X. H. Xia, J. P. Tu, J. Zhang, X. L. Wang, W. K. Zhang and H. Huang, *Sol. Energy Mater. Sol. Cells*, 2008, **92**, 628-633.
42. M. Chigane and M. Ishikawa, *J. Electrochem. Soc.*, 1994, **141**, 3439-3443.
43. D. Han, P. Xu, X. Jing, J. Wang, P. Yang, Q. Shen, J. Liu, D. Song, Z. Gao and M. Zhang, *J. Power Sources*, 2013, **235**, 45-53.
44. X. H. Xia, J. P. Tu, X. L. Wang, C. D. Gu and X. B. Zhao, *J. Mater. Chem.* , 2011, **21**, 671-679.
45. S. Vijayakumar, S. Nagamuthu and G. Muralidharan, *ACS Appli. Mater.Inter.*, 2013, **5**, 2188-2196.
46. A. K. Singh, D. Sarkar, G. G. Khan and K. Mandal, *J. Mater. Chem. A*, 2013, **1**, 12759-12767.
47. F. I. Dar, K. R. Moonooswamy and M. Es-Souni, *Nanoscale Res. Lett.*, 2013, **8**.
48. J. H. Zhu, J. A. Jiang, J. P. Liu, R. M. Ding, H. Ding, Y. M. Feng, G. M. Wei and X. T. Huang, *J Solid State Chem.*, 2011, **184**, 578-583.
49. Y. G. Zhu, G. S. Cao, C. Y. Sun, J. Xie, S. Y. Liu, T. J. Zhu, X. B. Zhao and H. Y. Yang, *Rsc Adv*, 2013, **3**, 19409-19415.
50. N. S. Liu, J. Li, W. Z. Ma, W. J. Liu, Y. L. Shi, J. Y. Tao, X. H. Zhang, J. Su, L. Y. Li and Y. H. Gao, *ACS Appli. Mater.Inter.*, 2014, **6**, 13627-13634.
51. K. Zhuo, M. G. Jeong and C. H. Chung, *Rsc Adv*, 2013, **3**, 12611-12615.
52. J. W. Zhao, J. Chen, S. M. Xu, M. F. Shao, Q. Zhang, F. Wei, J. Ma, M. Wei, D. G. Evans and X. Duan, *Adv. Funct. Mater.*, 2014, **24**, 2938-2946.
53. H. H. Nan, W. Q. Ma, Z. X. Gu, B. Y. Geng and X. J. Zhang, *Rsc Adv*, 2015, **5**, 24607-24614.
54. W. M. Zhang, J. S. Hu, Y. G. Guo, S. F. Zheng, L. S. Zhong, W. G. Song and L. J. Wan, *Adv Mater*, 2008, **20**, 1160-+.

55. Y. Q. Zou and Y. Wang, *Nanoscale*, 2011, **3**, 2615-2620.
56. B. Varghese, M. V. Reddy, Z. Yanwu, C. S. Lit, T. C. Hoong, G. V. Subba Rao, B. V. R. Chowdari, A. T. S. Wee, C. T. Lim and C.-H. Sow, *Chem. Mater.*, 2008, **20**, 3360-3367.
57. H.-W. Lee, P. Muralidharan, R. Ruffo, C. M. Mari, Y. Cui and D. K. Kim, *Nano Lett.*, 2010, **10**, 3852-3856.
58. L. Liu, Y. Li, S. M. Yuan, M. Ge, M. M. Ren, C. S. Sun and Z. Zhou, *J. Phys. Chem. C*, 2010, **114**, 251-255.
59. D. W. Su, M. Ford and G. X. Wang, *Sci Rep*, 2012, **2**.
60. A. Caballero, L. Hernan, J. Morales, Z. Gonzalez, A. J. Sanchez-Herencia and B. Ferrari, *Energ. Fuel.*, 2013, **27**, 5545-5551.
61. W. F. Yang, G. H. Cheng, C. Q. Dong, Q. G. Bai, X. T. Chen, Z. Q. Peng and Z. H. Zhang, *J. Mater. Chem. A*, 2014, **2**, 20022-20029.
62. Y. J. Mai, S. J. Shi, D. Zhang, Y. Lu, C. D. Gu and J. P. Tu, *J Power Sources*, 2012, **204**, 155-161.
63. Y. Huang, X. L. Huang, J. S. Lian, D. Xu, L. M. Wang and X. B. Zhang, *J. Mater. Chem.* , 2012, **22**, 2844-2847.
64. M. Y. Cheng, Y. S. Ye, T. M. Chiu, C. J. Pan and B. J. Hwang, *J. Power Sources*, 2014, **253**, 27-34.
65. J. H. Pan, Q. Z. Huang, Z. Y. Koh, D. Neo, X. Z. Wang and Q. Wang, *ACS Appli. Mater.Inter.*, 2013, **5**, 6292-6299.
66. X. F. Li, A. Dhanabalan and C. L. Wang, *J Power Sources*, 2011, **196**, 9625-9630.

**Figures and Captions:**

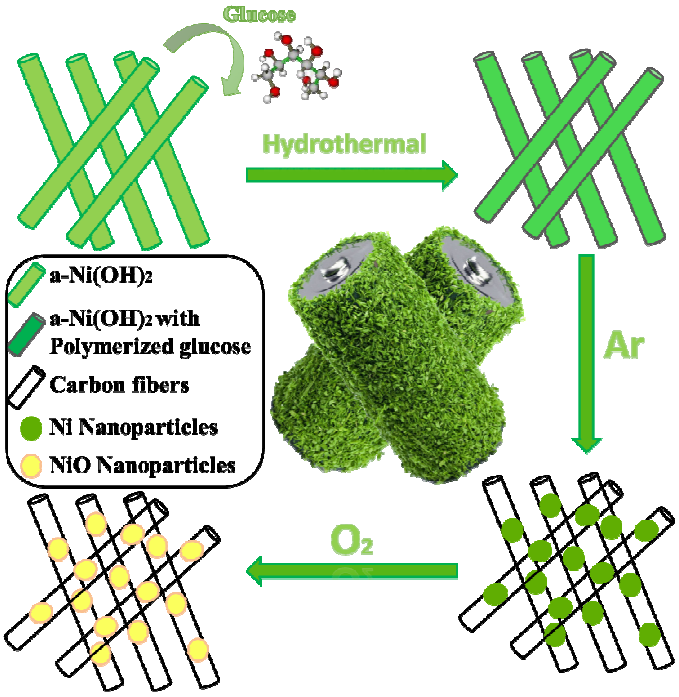


**Scheme 1** Schematic illustration to introduce the whole fabrication route from α-$Ni(OH)_2$ nanowires to peapod Ni/C and finally to peapod NiO/C. This unique structure can be considered as high-efficiency electrode in energy storage.

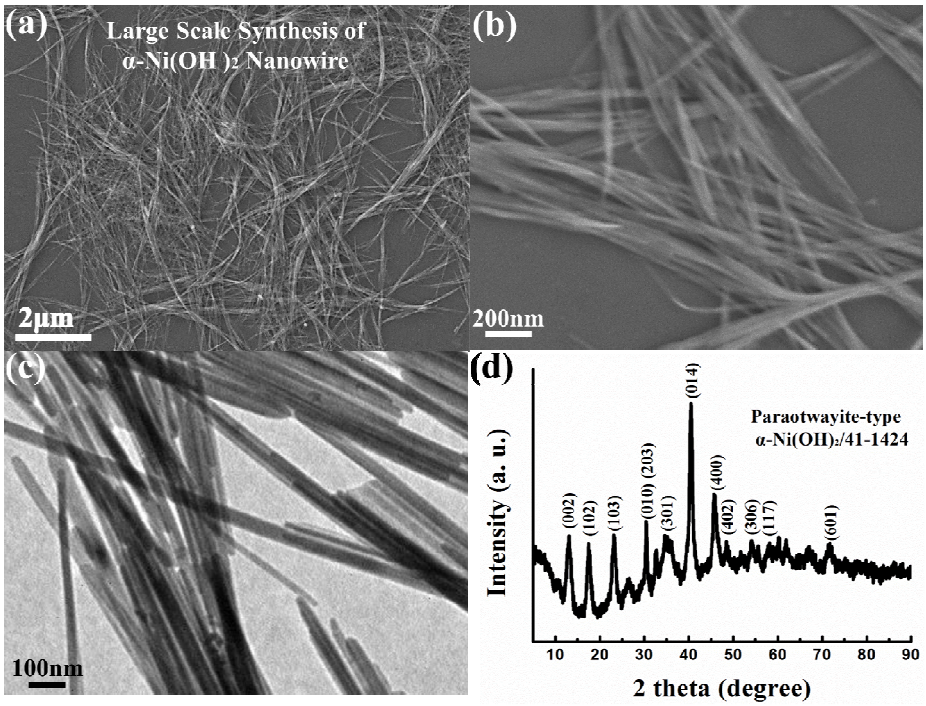


**Figure 1** General characterizations of α-$Ni(OH)_2$ nanowires. (a), (b) the SEM images in different resolutions. (c) TEM image. (d) XRD data.

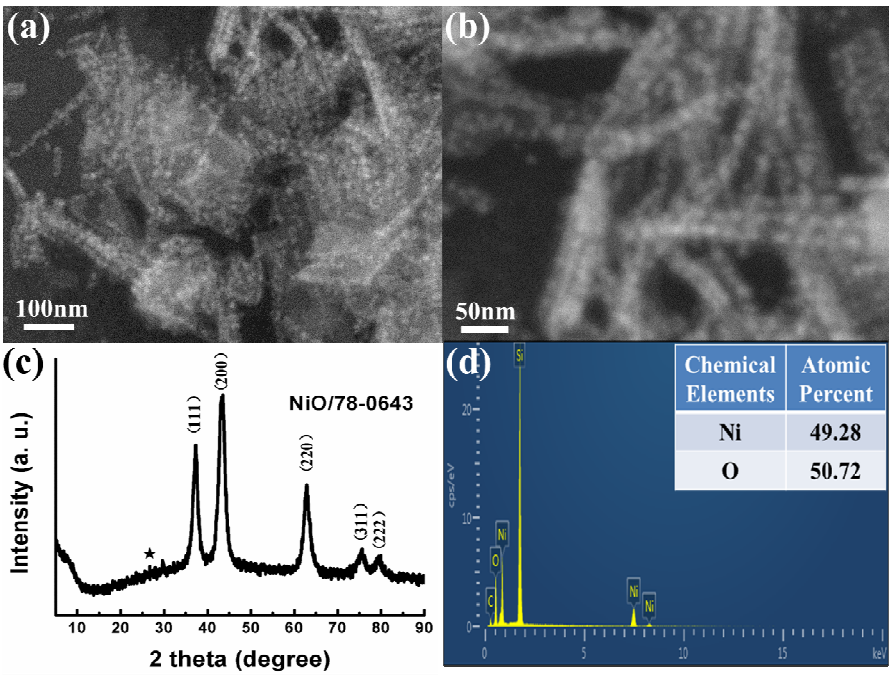


**Figure 2** SEM images at lower (a) and higher (b) resolutions to clearly demonstrate the peapod morphology. (c) XRD pattern of the peapod composite. (d) The corresponding EDS data.

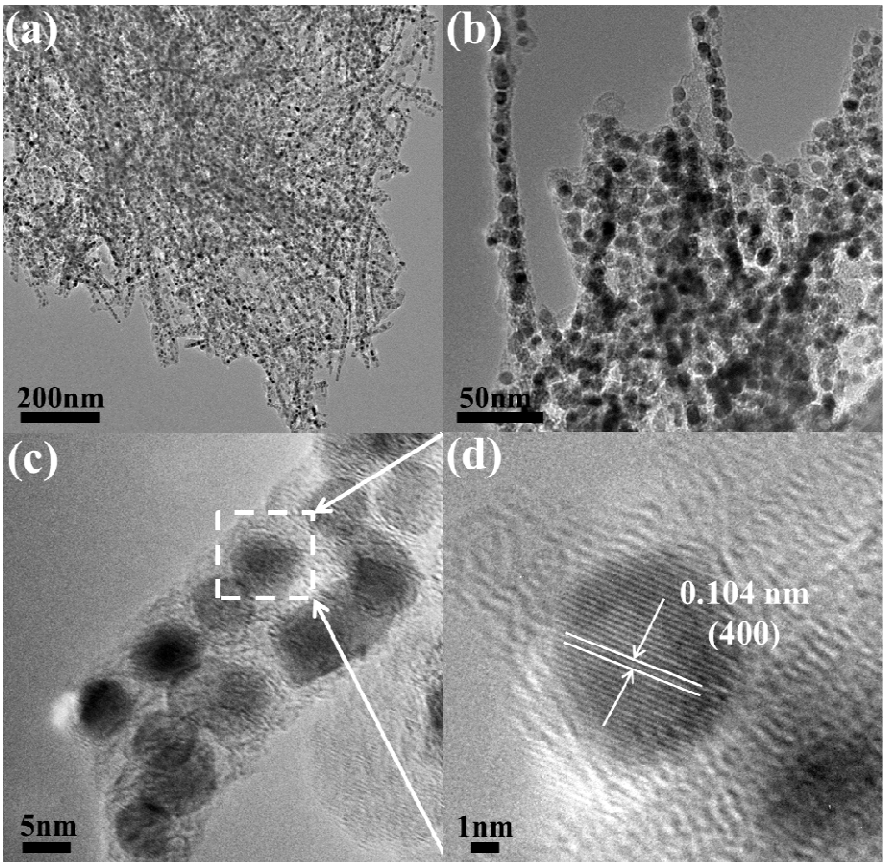


**Figure 3** (a) Low- magnification TEM image to confirm the large-synthesis of peapod NiO/C. (b) and (c) are the magnified TEM images to uncover structure details on a tiny scale. (d) HRTEM image to discover the crystal structure of NiO nanoparticles.

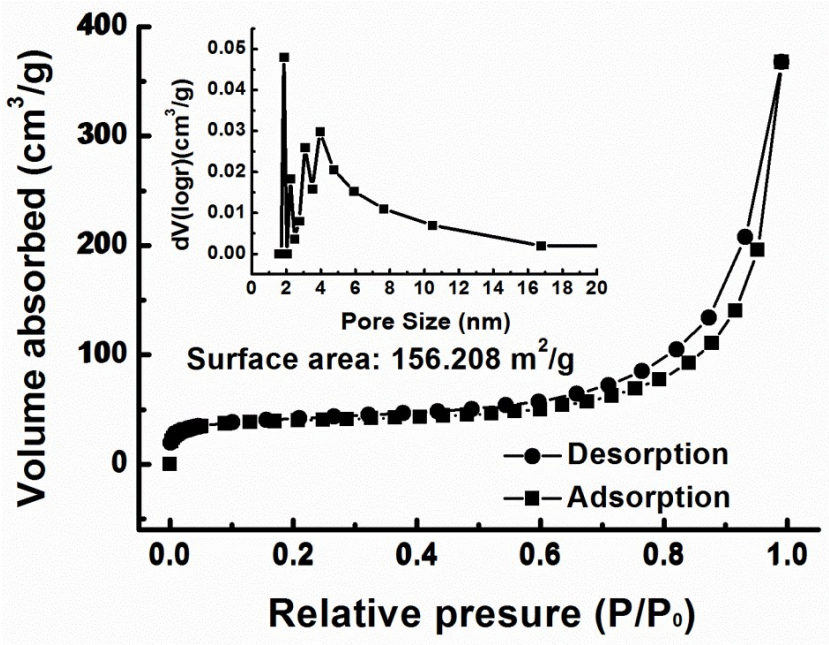


**Figure 4** BET profile of the peapod NiO/C to reveal the specific surface area and pore size distribution derived from the desorption branch (inset)

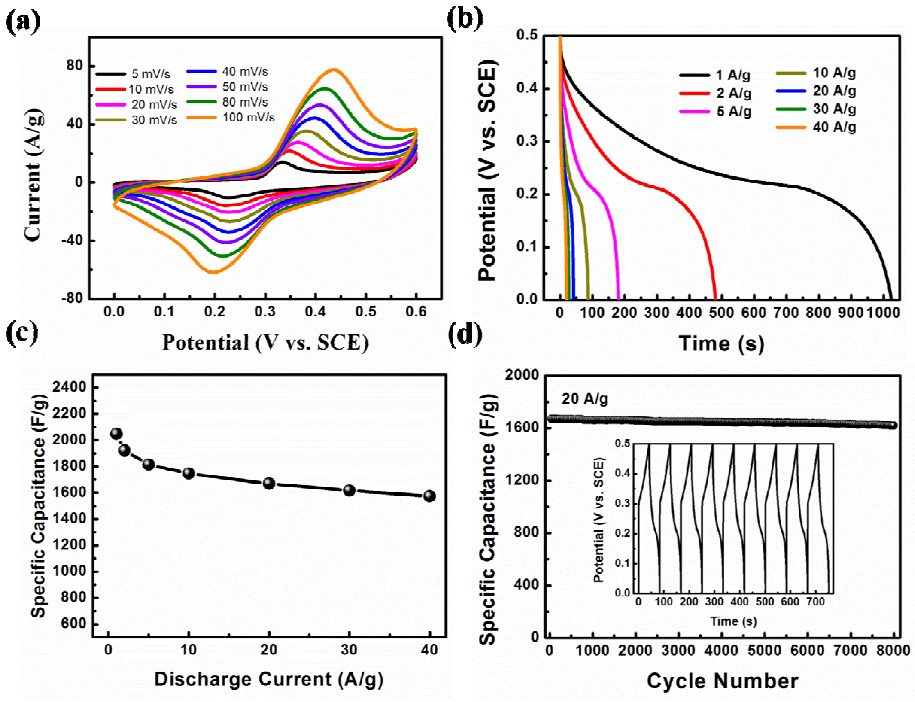


**Figure 5** Electrochemical performances of peapod NiO/C. (a) CV curves at various scan rates form 5 to 100 mV/s within the potential window of 0-0.6 V. (b) Galvanostatic discharge profiles at different densities from 1 to 40 A/g. (c) Current density dependence of the specific capacitance. (d) Cyclic stability at the current density of 20 A/g (inset: charge/discharge profiles at the rate of 20 A/g).

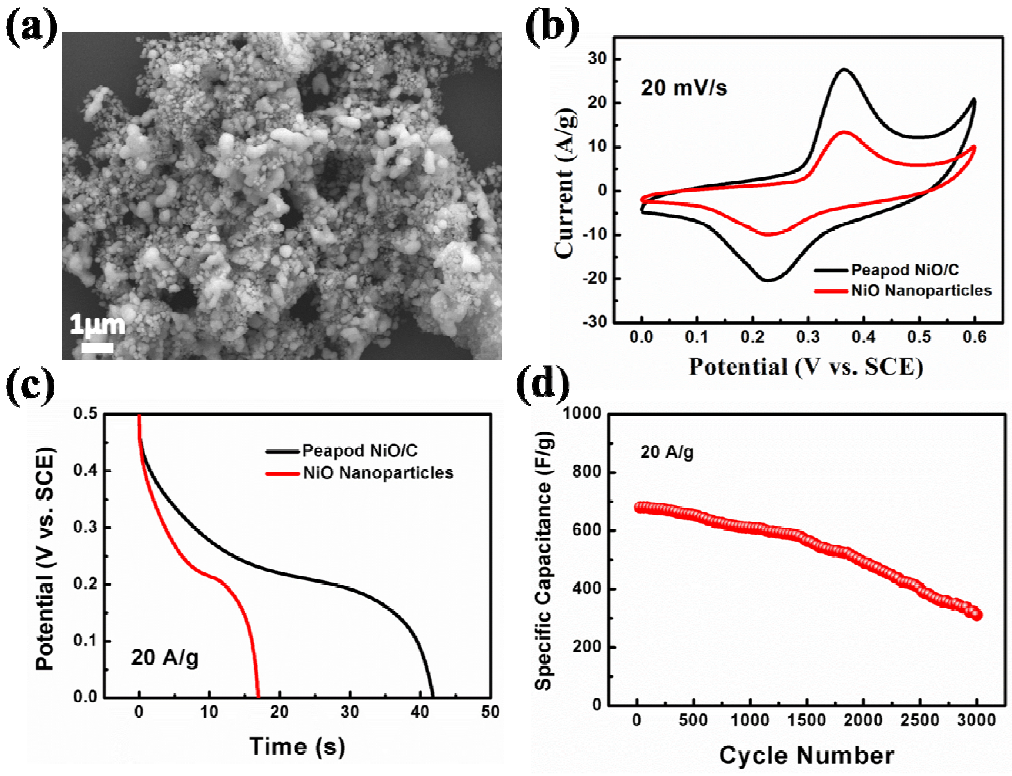


**Figure 6** Electrochemical performances of NiO nanoparticles for comparison. (a) SEM image. (b) CV curves and (c) discharge cycles of peapod NiO/C (black line) and NiO nanoparticles (red line), respectively. (d) Cyclic stability of NiO nanoparticles at 20 A/g for 3000 cycles.

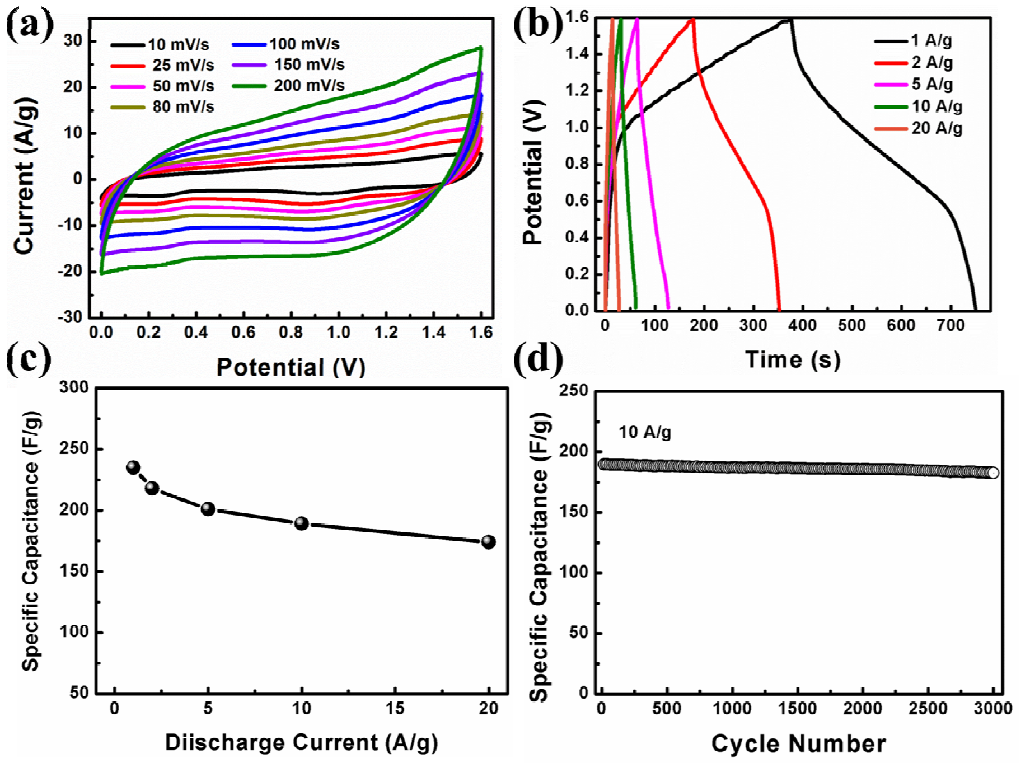


**Figure 7** Electrochemical performances of asymmertric supercapacitor (NiO/C//AC-ACS). (a) CV plots of the device tested at various scan rates of 10-200 mV/s from 0 to 1.6 V. (b) Galvanostatic charge/discharge profiles at different densities ranging from 1 to 20 A/g. (c) Rate performances calculated through discharge curves. (d) Cycling performance at the current density of 10 A/g.

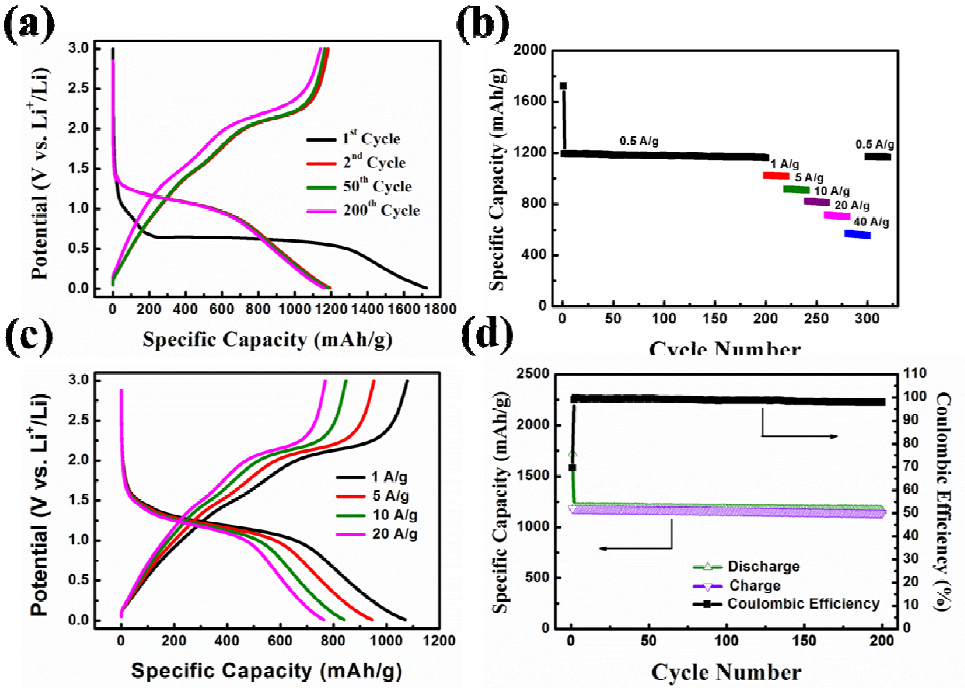


**Figure 8** Li storage performances of peapod NiO/C. (a) Galvanostatic charge/discharge curves at the current density of 0.5 A/g for 200 cycles. (b) Rate performances from 0.5 to 40 A/g and finally back to 0.5 A/g. (c) Galvanostatic charge/discharge curves of the second cycles at various current densities from 1 to 20 A/g. (d) Coulombic efficiency at the current density of 0.5 A/g.

| Morphology | Current (A/g) | Initial Capacitance (F/g) | Cycle Number | Capacitance retention (%) | Ref |
|---|---|---|---|---|---|
| **1 D Ni/NiO core/shell nano-heterostructures** | 8.6 | 1722 | 200 | 98 | 44 |
| **1D NiO nanorod** | 44 | 955 | 500 | 93 | 45 |
| **Nanoporous NiO film** | 10 | 940 | 1000 | 97 | 22 |
| **NiO nanowall arrays** | 1.6 | 238 | 4000 | 93 | 46 |
| **NiO Nanoflakes** | 10 ($mA/cm^2$) | 144 | 500 | 92 | 43 |
| **3D NiO/graphene** | 10 | 300 | 2000 | 79 | 8 |
| **NiO nanoflakes/graphene** | 5 | 100 | 1500 | 99 | 47 |
| **Ni@NiO Nanowire** | 0.512 ($A/cm^3$) | 36 ($F/cm^3$) | 3000 | 89 | 48 |
| **Dendritic nanoporous NiO** | 1 | 804 | 2000 | / | 49 |
| **Peapod NiO/C** | 20 | 1670 | 8000 | 97 | This work |

**Table 1** Supercapacitor performances of NiO-based materials with different morphologies reported in the previous literatures.

| Morphology | Current (mA/g) | Initial Capacity (mAh/g) | Cycle Number | Capacity Retention (%) | ref |
|---|---|---|---|---|---|
| **NiO Microspheres** | 50 | 1570 | 30 | 10 | 56 |
| **Facet Mesoporous NiO Nanosheets** | 717 | 1200 | 100 | 92.1 | 57 |
| **2D NiO nanoplate** | 100 | 1500 | 20 | 93 | 58 |
| **NiO Nanorod Arrays on Ni foam** | 717 | 1521 | 70 | 88 | 59 |
| **NiO–graphene hybrid** | 100 | 1115 | 35 | 86.3 | 60 |
| **NiO Nanowalls** | 448 | 1502 | 20 | 94 | 62 |
| **ultrathin porous NiO nanosheets/graphene** | 100 | 1398 | 50 | 85 | 61 |
| **Flowerlike Hierarchical NiO Microspheres** | 50 | 1295 | 5 | 89.7 | 63 |
| **NiO nanosheets/ graphene** | 71 | 1650 | 40 | 97.6 | 53 |
| **porous NiO–Ni nanocomposite** | 286 | 500 | 100 | 77 | 64 |
| **Peapod NiO/C** | 500 | 1723 | 200 | 97 | This Paper |

**Table 2** Li storage performances of NiO-based composites of different morphologies in the previous literatures.

**Table of Content**

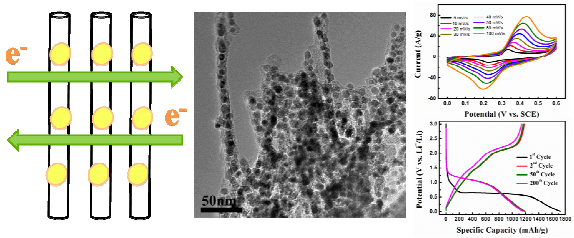


We report novel peapod NiO nanoparticles encapsulated in carbon fibers, which exhibits outstanding electrochemical performances in both SCs and LIBs.